Title

Manufacturing scalability implications of materials choice in inorganic solid-state batteries

Journal

Joule, 5(3)

ISSN

2542-4785

Authors

Huang, Kevin J
Ceder, Gerbrand
Olivetti, Elsa A

Publication Date

2021-03-01

DOI

10.1016/j.joule.2020.12.001

Peer reviewed

Manufacturing Scalability Implications of Materials Choice in Inorganic Solid-State Batteries

Kevin J. Huang[1], Gerbrand Ceder[2], Elsa A. Olivetti[1*]

[1]Department of Materials Science & Engineering, MIT, Cambridge, MA 02139; [2]Department of Materials Science & Engineering, University of California Berkeley, Berkeley, CA 94720, USA

Abstract

The pursuit of scalable and manufacturable all-solid-state batteries continues to intensify, motivated by the rapidly increasing demand for safe, dense electrical energy storage. In this Perspective, we describe the numerous, often conflicting, implications of materials choices that have been made in the search for effective mitigations to the interfacial instabilities plaguing solid-state batteries. Specifically, we show that the manufacturing scalability of solid-state batteries can be governed by at least three principal consequences of materials selection: (1) the availability, scaling capacity, and price volatility of the chosen materials' constituents, (2) the manufacturing processes needed to integrate the chosen materials into full cells, and (3) the cell performance that may be practically achieved with the chosen materials and processes. While each of these factors is, in isolation, a pivotal determinant of manufacturing scalability, we show that consideration and optimization of their collective effects and tradeoffs is necessary to more completely chart a scalable pathway to manufacturing.

Context & Scale

With examples pulled from recent developments in solid-state batteries, we illustrate the consequences of materials choice on materials availability, processing requirements and challenges, and resultant device performance. We demonstrate that while each of these factors is, by itself, essential to understanding manufacturing scalability, joint consideration of all three provides for a more comprehensive understanding of the specific factors that could impede the scale up to production. Much of the recent activity in solid-state battery research has been aimed at mitigating the various interfacial instabilities that currently prevent the fabrication of a low cost, high performance device. With such a wide breadth of options, it can be difficult for researchers to identify the most promising or scalable pathways forward. As such, we aim to empower researchers to make more informed decisions by providing them with insights into how their materials choices are likely to impact the manufacturing scalability of different interfacial mitigation alternatives. In doing so, we hope that generalizable lessons about scalability can be extracted and applied to subsequent challenges in solid-state battery development, thereby accelerating their scale up to manufacturing.

Introduction

The demand for electrical energy storage is widely anticipated to escalate over the coming years. Considerable growth in global renewable energy capacity and electrified mobility[1] necessitate an efficient, cost effective, safe, and large-scale means of storing energy. While the cost and performance of traditional lithium-ion batteries continues to improve[2], interest and effort in the development of all solid-state lithium batteries has been accelerating. By enabling the use of thin, high capacity lithium metal anodes and thin, solid electrolyte separators, solid-state batteries potentially provide for a higher energy density storage solution. Moreover, by eliminating the need for volatile liquid electrolytes, solid-state batteries could also offer a safer, more reliable alternative to current rechargeable batteries.

In the pursuit of sufficiently high performing solid-state batteries, a wide range of electrolyte chemistries and structural archetypes are under investigation: oxide-based garnets[3–8], LISICON-like (lithium superionic conductor) and argyrodite-type sulfides[9–19], NASICON-like (sodium superionic conductor) phosphates[9,11,12,14–16,20–26], and perovskites[11,12,14–16,20,21,23], among others. Given this range of options, how are promising pathways to large scale integration to be identified? The factors that can govern the manufacturability and scalability of materials dependent technologies, like batteries, are considerably varied[27]. This is further compounded during the transition from lab to production, as the challenges that confront battery scientists and engineers continue to evolve.

At present, the integration of solid electrolytes into full, solid-state battery cells remains largely an unsolved challenge. Much effort is currently being directed toward improving the numerous instabilities that continue to degrade the cathode and anode interfaces in these cells (high impedance, dendrite formation, interphase formation and interdiffusion, etc.)[28–46]. But as with the diversity of candidate solid electrolytes, a broad range of strategies has been reported in the literature to mitigate these interfacial problems. Much of this work, for example, has focused on stabilizing the interface between the solid electrolyte and lithium metal anodes through the use of artificial interlayers. Buffer layers have been incorporated through a variety of methods including liquid phase deposition[30,33,41–43,47], evaporation[32,33,39,40], atomic layer deposition[34,34,48], sputtering[35,38,49,50], powder pressing[44], and melt deposition[37]. Similar strategies have also been applied to improve the interface between cathode active material particles and various solid electrolytes. Very thin layers of certain oxides, for instance, have been applied to cathode particles to stabilize their interfaces with sulfide solid electrolytes[51–57]. Likewise, lithium borates have been found to provide a low melting point, high conductivity, and high bonding material to improve the interface between cathode active materials and garnet electrolytes[28,29,58,59] under their required processing conditions.

This considerable materials diversity affords us the opportunity to examine how materials selection could potentially impact manufacturing scalability. We thus review and analyze a selection of literature-reported, solid-state batteries employing varied interfacial mitigation approaches and materials to show that the manufacturing scalability of solid-state batteries is driven, at least in part, by: (1) the availability, scaling capacity, and price volatility of the chosen materials' constituents, (2) the manufacturing processes prescribed by the properties of the chosen materials, and (3) the specific capacities that can be extracted from the chosen materials in practice. We find that exploration of any of these factors in isolation may miss critical aspects of battery scalability. Rather, the numerous, sometimes diverging, consequences of materials choice in solid-state battery design must be collectively evaluated such that their combined effects and tradeoffs are considered.

Materials and Availability

Due to the dominant role of materials costs in overall solid-state lithium battery cost[60,61], supply chains for the various required electrolyte precursors must be rapidly developed such that their production costs fall by several orders of magnitude. Lab scale pricing for many of these precursors remains in the thousands or tens of thousands of dollars per kg (at the proper purities). To reach the manufacturing scale materials cost assumptions employed in this analysis, however, electrolyte precursor costs will have to be reduced by approximately 100x. While this may be achievable for some of the relevant precursors in the near term, sizeable deployment of solid-state batteries relying on a single electrolyte chemistry may ultimately be constrained by the inability of precursor materials supply chains to achieve sizable economies of scale[62].

A key determinant of materials cost is the actual or perceived availability of the elements that constitute that material's precursors. Given this, we evaluated the availability of several key constituents of three common solid-state electrolytes: $Li_7La_3Zr_2O_{12}$ (LLZO), $Li_{10}GeP_2S_{12}$ (LGPS), and Li_6PS_5Cl. Our initial screening of their availability produced a list of five, potentially constrained, elements: Ge, La, Nb, Ta, and Zr. We acknowledge that additional elements other than those included here (Ta, Nb) are sometimes used

throughout the literature to dope LLZO—Al, Ca, Ga, and Tb, for example. However, using our natural language processing pipeline[63–66], we have determined that Ta-doped LLZO remains the most frequently reported variant (the full LLZO corpus used in our analysis can be found online at synthesisproject.org), likely due to its comparatively high ionic conductivity and processability[41]. Recent analysis of the literature by Mahbub, et al., has likewise revealed that c-site modification (of which Ta-doping is one example) of similar lithium garnets is correlated with reduced processing temperatures while still being able to maintain suitably high ionic conductivities[67]. We, therefore, focus our present analysis on Ta-doped LLZO as reported in the work by Han, et al[29]. While cathode active materials cost constitutes large fractions of cell cost, we refer the reader to prior work done in this area[68] and instead focus here on the availability of electrolyte and interfacial mitigation materials.

To evaluate materials availability, we examined the viability of significant scale up in the production of Ge, La, Nb, Ta, and Zr, as informed by expected electric vehicle (EV) growth (method and full analysis provided in Supplemental Information). Based on our initial screening, we find no major concern associated with Nb or Zr. Ge and Ta, however, required further investigation (La raises minor availability concerns, but due to data availability, we focus on Ge and Ta in our analysis). At a battery production volume of 100 GWh/yr (annual EV production in 2030[69–71]), production of these critical elements must scale to 120 and 22 times their 2018 production, respectively[72].

Both Ge and Ta are mined as by-products, metals mined and produced from the extraction of other materials. Ge is produced as a by-product of coal ash and Zn, while Ta results from the production of Sn and Nb. The supply of these by-products is contingent on the dynamics of their carrier materials[73]. When prices of by-products increase, but not those of the carriers, dedicated increases in carrier production is not typically expected (assuming that production economics are driven by the price of the carrier), effectively constraining the supply of the by-products. To gauge this, supply potential is used, the maximum by-product content accompanying the production of the carrier[74]. This provides an upper bound to the by-product supply that could be obtained without a dedicated increase in carrier production. The supply potentials of Ge and Ta are presented in Fig. 1.

Chiefly produced in China, Ge is a by-product of the processing of Zn ore, which is initially recovered by leaching Zn-refining residues or coal ash, precipitating concentrate from this leachate (to $GeCl_4$), and then hydrolyzing the concentrate to produce GeO_2[75]. As the precursor commonly used to synthesize Ge-containing solid-state electrolytes (such as LGPS) is GeS_2, the obtained GeO_2 must then undergo further processing. Unfortunately, however, less than 5% of the Ge contained in Zn concentrates ever reaches refineries capable of extracting and producing Ge as described. The Ge supply potential from Zn and coal ash is compared to Ge production from 1960-2018 in Fig. 1a. We see that the total potential supply of Ge from Zn and coal is 100x what is currently produced. Accordingly, while the elemental availability of Ge is not in question, facilities that can process this material are limited. Whether this capability can be rapidly expanded will no doubt be dictated by profit maximization and environmental regulations. Moreover, any aggressive increase in Ge processing capacity will also surely impact Ge price and, hence, LGPS cost. Given these logistical constraints, Ge recycling from recovered scrap, which currently accounts for 30% of world production, will need to play a more significant role.

Ta is derived as a by-product of Sn and Nb (two materials that, by themselves, are also relevant to solid-state battery production), with the relevant Ta-containing precursor being Ta_2O_5. A significant fraction of Ta material trade is undocumented, as leading ore and concentrate producers rely on artisanal mining operations, a recovery mode that has historically led to supply constraints. As presented in Fig. 1b, the supply potential of Ta from Sn and Nb is less than double current production, indicating that Ta production would, therefore, fail to meet projected increases in demand driven by the scale up of solid-state batteries.

However, sizeable Ta resources exist in Australia and Brazil, resources that are not currently being exploited. Interestingly, Ta could also be recovered as a by-product of Li from spodumene production in Australia and Canada, further entangling the supply chains of these various battery-relevant materials.

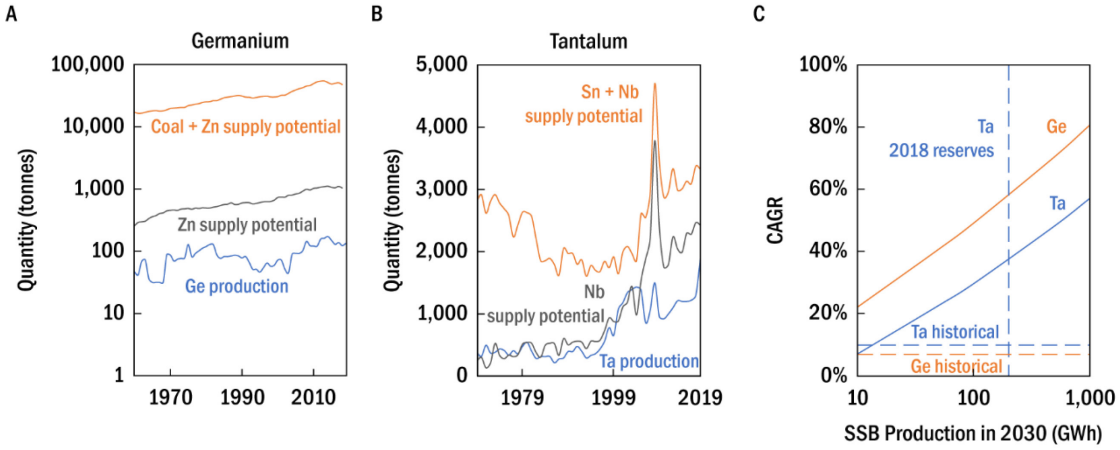

Fig. 1. Materials availability and scaling requirements for Ge and Ta
(a) Supply potential for Ge from dominant carrier metals compared with current production. (b) Supply potential for Ta from dominant carrier metals compared with current production. (c) Compound annual growth rate (CAGR) needed to achieve a given solid-state battery production volume in 2030 in GWh. Vertical dashed line corresponds to Ta reserves in 2018. Horizontal dashed lines indicate maximum historical CAGRs.

The considerable scaling required of Ge and Ta production prompts consideration of the staggering impact this will have on the supply chains of compounds containing these elements. Fig. 1c presents the required compound annual growth rate (CAGR) in metal production as a function of solid-state battery production in 2030 for each of these elements. The required quantity of each element is determined by a materials intensity that has been calculated based on electrolyte stoichiometry, electrolyte usage in the battery, and literature-reported battery capacity (details in Supplemental Information). The calculated CAGRs for Ge and Ta (Fig. 1c) to meet the projected surge in EV production far exceed their respective historical growth rates[76]. The average 18-year CAGRs for Ge and Ta since 1972 are 1% and 4%, respectively (with maximum CAGRs of 7% and 10%, respectively). For 100 GWh/yr of annual solid-state battery production in 2030, the required CAGRs for Ge and Ta are ~50% and ~30%, respectively. Such unprecedented growth rates are likely to significantly impact the cost of all solid-state model cells discussed throughout this Perspective except for those based on argyrodite-type electrolytes. The vertical dotted line in Fig. 1c indicates the 2018 reserves limit for Ta (reserves are the quantity which could be extracted or produced at the time of determination). As can be seen, for the projected growth in battery production, the possible short-term scarcity of Ta and subsequent availability-driven price increases could considerably impede the scale up of solid-state batteries based on Ta-doped variants of LLZO (in contrast, reserves and resources for Ge are found to be sufficient). Recycling could begin to play a role in meeting this demand. However, previous work indicates this role will likely be limited until 2040 due to vehicle and battery lifetimes[77]. As researchers explore the use of particular materials, screening analyses can enable them to understand how the scaled resource use will impact primary supply based on the fraction of total end-use demand that the new application requires[78].

Given the lack of available data, we assumed a constant electrolyte price ($50/kg[60,61]) across the model battery cells used throughout our analysis; this would not be the case in practice, however. Ge and Ta are extremely high priced elements, exceeded only by Au, Sc, and platinum group metals (50-year average[79]). Moreover, both elements have exhibited high price volatility as well. Ta, for example, has a recent price volatility of 40% (price variation of 40% of its mean over a 5-year period), driven by increased use in electronics applications. Similarly, Ge has exhibited a 30% 5-year average volatility. The scale up of solid-state batteries, therefore, may potentially be hindered not only by the logistical and operational barriers to scaling the requisite precursor materials supply chains at unprecedented rates, but by the price uncertainty and volatility of these high-priced elements as well.

Materials availability constraints are provide a significant source of uncertainty that will drive the total cost of solid-state batteries. As has been previously noted for existing battery technologies, the dominance of materials in the cost structure may set a practical lower bound on battery price[80]. However, as materials choices will, in turn, dictate the manufacturing processes that can or must be used, we consider the implications of these choices on cell processing as well.

Materials and Processing

One of the key differences between sulfide and oxide solid electrolytes is the disparity in their elastic moduli, with sulfide solid electrolytes typically exhibiting moduli an order of magnitude lower than those of their oxide counterparts[10,81–83]. This key difference in electrolyte materials properties has several consequences. First, sulfide electrolytes may be better able to accommodate the volume changes that accompany repeated charge and discharge cycles in an all-solid-state cell, thereby maintaining superior solid-solid interfacial contact across the lifetime of the battery[84]. However, this potentially enhanced ability to withstand cycling-induced stresses could be offset by the lower fracture toughness of such materials, a vulnerability that makes them especially sensitive to flaws and defects that may be introduced during processing[83]. Second, the contrasting mechanical behavior between oxides and sulfides allows for sulfide sheets to be densified and bonded to device stacks through high pressure calendering, while oxide sheets must instead be sintered at high temperature for densification and adhesion, a critical process barrier that can chemically degrade the interface with other materials, especially cathode active materials[28]. Third, while the lower modulus of sulfide electrolytes might enable very thin, large area sheets of these materials to better withstand the rigors of large scale manufacturing[85,86], higher modulus oxide sheets might be more prone to failure under the requisite large scale handling and processing conditions. Thin, large area, tape cast sheets are well known to warp, crack, shrink, and delaminate upon heating, particularly when the slurry composition and its processing conditions are not properly optimized[84–98], making higher modulus oxide sheets especially vulnerable to failure during their required high temperature sintering.

The consequences of this disparity in mechanical properties is not trivial. And while the processing-driven uncertainty in the ability of sulfide electrolytes to better withstand cycling stresses demands examination, it is a question that currently lies outside the scope of our models. Instead, we analyze how the difficulty of processing and handling extremely thin, large area, oxide electrolyte sheets could manifest by modeling the possible manufacturing costs of two hypothetical cells informed by the work by Han, et al.[29] Our analysis is motivated, in part, by the apparent difficulty in producing solid-state batteries based on thin, garnet separators at high yield, even in industry[99–105]. In our model cells, $Li_{2.3-x}C_{0.7+x}B_{0.3-x}O_3$ (LCBO) is used in the composite cathode as a low melting point, high binding, and suitably conductive "solder" at the interface between cathode active material ($LiCoO_2$, LCO) and solid electrolyte particles (Ta-doped LLZO). Given that the solid electrolyte separator must be sintered at high temperature, it must be cast, dried, cut, and sintered by itself first, with the much thicker composite cathode subsequently cast and processed on top (this cell is referred to in our model as the "LLZO-LCBO" cell). However, at the low separator thicknesses (here, 20 μm) required to capture the desired energy density benefits of solid-state batteries, the

handling and processing of brittle oxide sheets with areas exceeding 100 cm^2 can be difficult. Accordingly, prior work proposes an alternative processing approach. First, a thick, porous oxide electrolyte framework (a "catholyte") is cast. Because it is 100 µm in thickness, researchers posit that it may be more easily handled and manipulated as a free-standing sheet than a 20 µm sheet of the same material[60,106]. The thin electrolyte separator is then cast on top, and the two are cut and sintered together before cathode active material is backfilled or infiltrated into the porous electrolyte framework. This variant of the LLZO-LCBO cell will be referred to as the "porous LLZO-LCBO" cell. Details for these cells (and the other subsequent model cells presented throughout this Perspective) as well as an overview of our cost modeling approach are presented in the Supplemental Information. We note, however, that our manufacturing cost calculations for each model cell are based on specific, literature reported cell design and performance data. This enables us to map individual cell design and materials choices to their resulting cell capacities and, as a consequence, their attendant manufacturing costs. The challenge with this modeling approach, however, is that the calculated costs of cells whose performance data were recorded at different testing conditions are not directly comparable. A cell discharging 100 mAh/g at low rate and high temperature does not have the same performance as a cell discharging 100 mAh/g at high rate and low temperature. Yet, with equivalent materials and processing, these two cells would be calculated to have equivalent manufacturing costs in $/kWh (we elaborate on the implications of this in the Supplemental Information and later in this discussion).

In Fig. 2a, we illustrate the manufacturing cost of the LLZO-LCBO cell as a function of process yield (used here as a proxy for process difficulty, with higher yield representing greater processing ease) for each of the indicated process steps. The effects of yield are studied for four key processing steps in LLZO-LCBO cell assembly: separator coating and drying (step 2), separator sintering (step 5), cathode printing (step 7), and cathode heating (step 8). Steps are numbered with their positions in the overall manufacturing process flow (process flows for all our model cells are presented in Table S1). A fifth curve that illustrates how simultaneous changes in yield to all four of these process steps impacts cell cost is presented as well. These particular process steps were chosen, as tape cast sheets have been found to more likely fail during forming and heating operations.

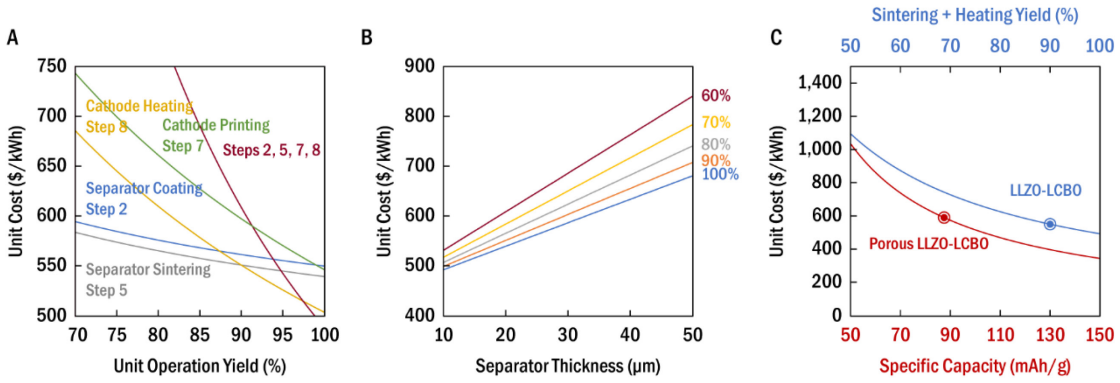

Fig. 2. Effects of process difficulty
(a) Manufacturing cost as a function of unit operation yield for key processing steps in the fabrication of the LLZO-LCBO cell. (b) Manufacturing cost as a function of separator thickness and separator sintering yield. (c) Manufacturing cost as a function of separator sintering + cathode heating yield for the LLZO-LCBO cell vs. manufacturing cost as a function of cell capacity for the porous LLZO-LCBO cell. Dots indicate baseline model values for each cell. Each x-axis corresponds to only the curve with the matching color. Specific capacity is based on active material mass in the cathode.

Our results indicate that modest drops in the yield of even a single process step can considerably increase the overall manufacturing cost of these cells. The effect of decreases in separator sintering yield, as one might expect due to the failure of these thin, large area, brittle oxide sheets during high temperature processing, is somewhat dampened by the relatively early position of the separator sintering step in the manufacturing process flow. In contrast, manufacturing cost is notably more sensitive to the yield of the cathode heating step. For example, a 5% drop in cathode heating yield from its baseline value results in a cost increase of ~$30/kWh, a nontrivial increase considering that a commonly accepted target cost for such batteries is $100/kWh[107,108]. Given the late position of cathode heating in the overall process flow—and its position after other low yield process steps, like separator sintering—failures during cathode processing have comparatively larger impacts. For example, when cells are lost during cathode heating, both composite cathode material and solid electrolyte separator materials are lost, representing a significant fraction of overall cell cost (see Fig. S1). In addition, many more sheets must be made in the numerous preceding process steps to accommodate these losses late in the process flow. Unsurprisingly then, the sensitivity of manufacturing cost to process yield is even more pronounced when the yield of all four critical heating operations is varied (Steps 2+5+7+8 in Fig. 2a).

Thus, while the difficulty of obtaining, processing, and handling thin, large area, standalone oxide electrolyte sheets could result in large increases in manufacturing cost, it is even more crucial that downstream process steps maintain high yield. Achieving high yield during cathode heating, for example, could be particularly difficult, as the device stack at this point in the process flow contains both the solid electrolyte separator as well as a thick composite cathode, a complex mixed materials system with a variety of solid-solid interfaces that could be especially vulnerable to thermally induced stresses and defects. Mitigating such processing-induced flaws, especially at the interfaces, will no doubt be integral to ensuring low unit production costs and high resulting device performance.

With the production cost of LLZO-LCBO cells so dependent on the yield of even just a few, key process steps, serious consideration must be given to alternative manufacturing strategies. For instance, it is potentially appealing to simply use a thicker solid electrolyte separator that can be cast and sintered with greater success (i.e., higher yield). However, given the sensitivity of cell manufacturing cost to separator thickness (shown as a function of separator sintering yield in Fig. 2b), such a simplistic strategy might not offer a clearly advantageous alternative. Take, for example, a scenario in which a 20 μm separator can be sintered with a yield of 80% and a separator with twice that thickness that can be sintered with a yield of 100%. Despite the considerable increase in process yield that is captured when using a thicker separator, the increase in solid electrolyte materials usage and the concomitant decrease in cell energy density result in a nearly $70/kWh net increase in total cell production cost.

The hypothetical fabrication of our porous LLZO-LCBO cell also potentially offers a more easily processed alternative. Despite the promise of easier manufacturing, however, reports of similar devices in the literature reveal an essential uncertainty. How successfully can cathode active material be backfilled or infiltrated into a thick, porous, solid electrolyte framework? Given that battery performance hinges on the quality of these solid-solid interfaces[84], ensuring intimate contact between cathode active material and solid electrolyte across their entire interfacial area is imperative. In one report, for example, a similar porous LLZO device structure was made. Active material precursor solution was then backfilled into the porous electrolyte[109]. It was necessary to repeat this process several times to achieve the desired active material loading. Ultimately, solid-state cells produced in this way could not be extensively cycled. Moreover, while this report illustrates the challenges attendant to a manufacturing approach that relies on the backfilling of cathode material into a porous electrolyte, doing so at production scale and speed and with the cathode slurry modeled here instead of the reported precursor solution could be more difficult.

To examine the tradeoffs between the production of the LLZO-LCBO cell and that of the porous LLZO-LCBO cell, we compare the manufacturing costs of each in Fig. 2c. The production cost of each cell is plotted as a function of each cell's key processing uncertainty. That is, the cost of the LLZO-LCBO cell is plotted as a function of the process yields for its separator sintering and cathode heating steps (similar to the analysis presented in Fig. 2a), while the cost of the porous LLZO-LCBO cell is plotted as a function of cell specific capacity. In this latter case, capacity is used as a proxy for the quality of the backfilled cathode-electrolyte interface, given the critical role that maintaining solid cathode-solid electrolyte contact has in cell performance[84].

As shown in Fig. 2c, the production cost for a porous LLZO-LCBO cell varies markedly with the resulting capacity of the cell, similar in magnitude to the sensitivity of LLZO-LCBO cell cost to sintering and heating process yield. The dots on each curve represent their baseline values in our models (for both cells, capacity = 87 mAh/g, sintering + heating yield = 90%), as informed by the literature[29,60]. Accordingly, at these baseline values, neither approach appears universally preferable to the other. Rather, a tradeoff between processability and cell performance exists. The LLZO-LCBO cell will be favored if it is more difficult to successfully and intimately backfill active material into the porous LLZO-LCBO cell (thus resulting in decreased cell capacity) than it is to handle and process thin, large area, brittle oxide electrolyte sheets (thus resulting in decreased process yield).

We note that an alternative use of thick, porous electrolyte layers has been described in the literature. Rather than infiltrating such porous electrolyte layers with cathode active material, they can, instead, be backfilled with lithium metal to form a composite anode[110–112]. As with the use case described in Fig. 2, the initial fabrication of a thick, porous oxide electrolyte layer provides for a potentially more easily manufacturable cell. Moreover, the electrolyte's porosity can also serve to accommodate the large volume changes that are expected to occur at the anode during cycling. While employing a thicker composite anode than would otherwise be used in an ideal cell structure (e.g., using a thin, lithium foil anode, as our model assumes) reduces the achievable energy density, this could, in fact, be outweighed by an even more substantial increase in manufacturability afforded by the cell design.

The preceding discussion has revealed that not only do materials choice and materials properties dictate the processes that can or must be used (e.g., calendering vs. sintering) as well as the challenges that could detrimentally impact the yield and, hence, cost of those processes (e.g., failure during heating), but that these considerations must ultimately be weighed against the performance that can be extracted from those materials in order to make meaningful determinations about scalability.

Materials and Performance

While materials and processing are key drivers of manufacturing scalability, how they combine to yield device performance is equally as critical. Battery cost models of the type used here frequently rely on a constant, theoretical or ideal cell capacity and a generalized cell configuration when evaluating manufacturing cost. As such models are typically being used to inform process and production facility optimization at scale, the use of such standards and simplifications to capture the maximum attainable performance (or lowest manufacturing cost) for a finalized device is entirely appropriate. However, as our goal here is to illustrate the scalability implications of various material and interfacial mitigation options currently being investigated in the research literature, our model requires separate performance data for each specific device design. That is, rather than using a theoretical or standard specific capacity for the cathode active materials used in our model batteries, we must instead map the literature reported cycling data for the cells on which our models are based to the specific materials and processing that produced those results (including, for example, specific choices for the electrolyte separator, composite cathode

compositions, and whatever interfacial mitigations or buffer layers were required to achieve the reported cell performance).

In Fig. 3a we present the manufacturing cost as a function of cell specific capacity for two sulfide-[43,44] and one argyrodite-based[113] model batteries that represent an illustrative diversity of interfacial mitigation strategies. In the first sulfide-based model cell, the lithium anode is treated with phosphoric acid to enhance its chemical stability with the LGPS electrolyte. This cell will be referred to as the "LGPS-acid" cell. In the other, a Sn-substituted version of the argyrodite electrolyte Li_6PS_5I is introduced as a stabilizing anode interlayer (subsequently referred to as the "LGPS-argyrodite" cell). A third, argyrodite-type cell using a Li_6PS_5Cl electrolyte is modeled. In this example, no additional anode interfacial material is introduced, but the study on which our model is based investigated the effect of binder content in the composite cathode. This cell will be referred to as the "LPSCl" cell.

Cost is a strong function of cell specific capacity. Even modest decreases in extracted capacity (e.g., ~10 mAh/g) can result in cost increases of nearly $50/kWh. When the commonly accepted target cost for these batteries is $100/kWh[107,108], such large increases in manufacturing cost can be ill afforded. Given these literature reported cell capacities, for solid-state batteries to be scalable, significant additional gains in performance must be captured with extremely low additional materials and processing costs.

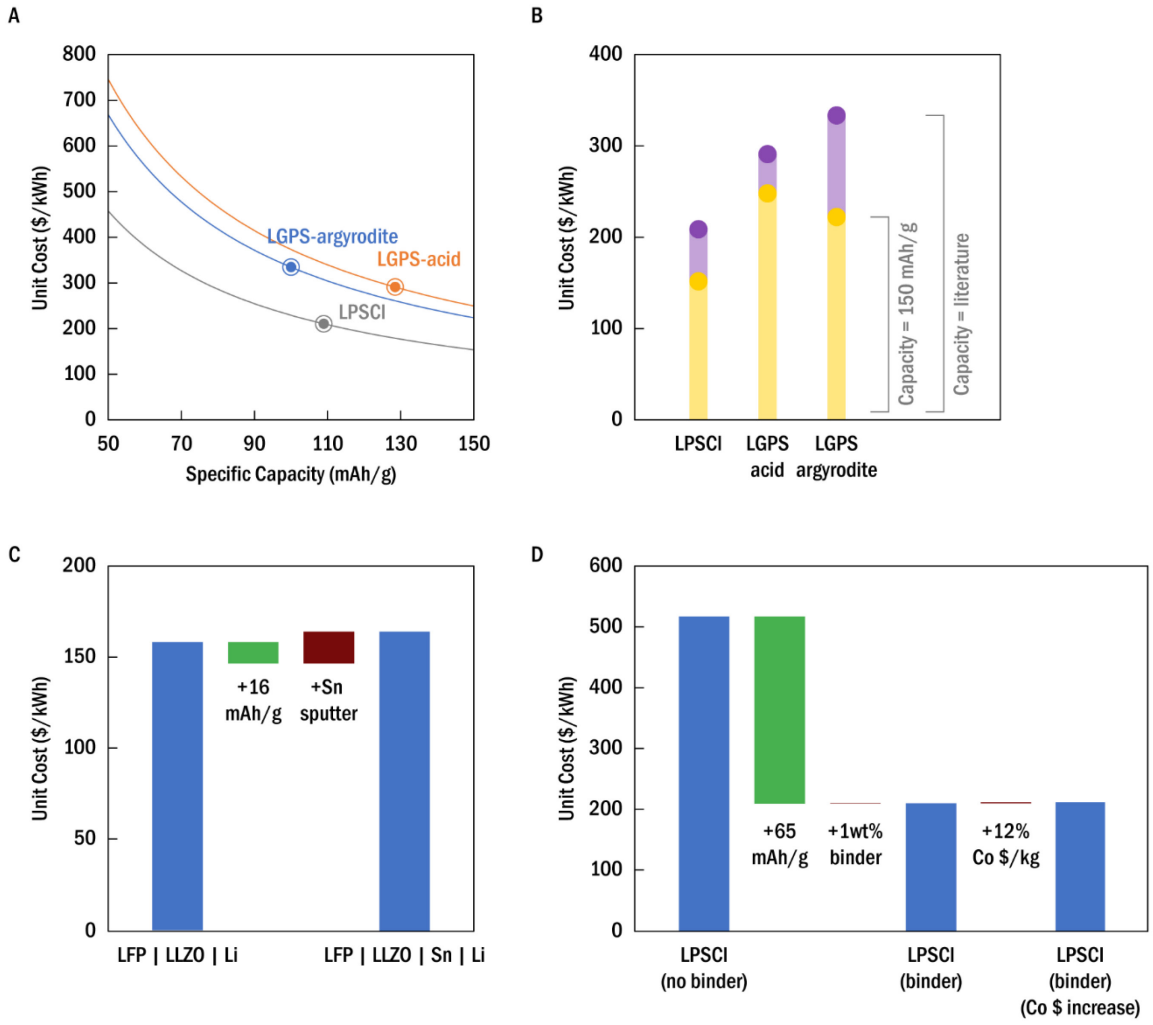

Fig. 3. Tradeoff between cell performance and cell processing cost
(a) Manufacturing cost of each model cell as a function of cell specific capacity. Dots indicate baseline model values for each cell. (b) Manufacturing cost as a function of their literature-reported specific capacities (purple dots) as well as a higher, hypothetical benchmark capacity of 150 mAh/g (yellow dots). The latter is used to isolate cost differences due only to underlying differences in materials and manufacturing, rather than differences in cell performance as well. (c) Manufacturing cost of an LFP | LLZO | Li cell utilizing a sputtered tin interlayer at the anode. Presented as a waterfall plot to illustrate the cost savings due to an increase in capacity upon insertion of the Sn interlayer as well as the cost increase due to the cost of sputtering the Sn interlayer itself. The manufacturing cost of this cell cannot be directly compared (in absolute terms) to that of our other model cells given that its high reported capacity relies on the use of small amounts of liquid electrolyte at the cathode-separator interface. Moreover, as this volume was unspecified in the report, it has also been excluded from the cost. (d) The LPSCl model cell discussed throughout this Perspective. Presented as a waterfall plot to illustrate the cost savings due to an increase in capacity upon the addition of 1 wt% binder to the composite cathode as well as the cost increase due to the cost of including 1 wt% binder in the composite cathode. Also illustrated is the effect of a 12% increase in the price of cobalt. Specific capacity is based on active material mass in the cathode in (a)-(d).

The substantial impact of cell capacity on manufacturing cost and, critically, the importance of using cell performance data that is specific to each device design and interfacial mitigation strategy is further examined in Fig. 3b. Here, cell cost is presented as a function of both the literature-reported specific capacity for each cell (purple dots) as well as a higher, hypothetical, benchmark cell capacity = 150 mAh/g (yellow dots). Differences in cost among the three cells using their literature-reported capacities reflect both differences in the materials and processing used to construct each cell as well as differences in the observed cell capacities. However, when each cell is set to a standard capacity of 150 mAh/g in our cost models, the remaining differences in cost between the various cells reflect only the underlying disparities in cell materials and manufacturing. For instance, while the LGPS-argyrodite cell is, nominally, more costly than the LGPS-acid cell, when both cells are set to the same, hypothetical benchmark capacity, the cost of the LGPS-argyrodite cell becomes lower than that of the LGPS-acid cell. This is because treatment with phosphoric acid is a costlier solution to anode interfacial chemical stability than the use of a thin argyrodite interlayer, due to both higher materials costs as well as higher processing costs. Despite this, because the LGPS-acid cell outperforms the LGPS-argyrodite cell, the total cost of the LGPS-acid cell is, in reality, lower. In other words, while it uses a costlier interfacial modification process (see Fig. S1(b)), the LGPS-acid cell captures enough additional cell performance to ultimately offset this cost premium and produce the more cost attractive cell design. Crucially, this underscores the need to consider the materials and processing costs of the cell as well as the literature reported performance that results from those specific materials and processing choices when evaluating battery scalability.

These examples illustrate a critical tradeoff in cell design: while it is possible to employ materials and process solutions that increase cell capacity, it is also possible that the additional materials and processing costs to incorporate those solutions can, in fact, offset any captured gains in cell performance. Both factors must be considered and balanced. In applying solutions to the challenges that currently plague solid-state batteries, gains in performance must far outstrip attendant gains in manufacturing cost.

Fig. 3c and 3d present this central tension with two contrasting examples. In the first, data is taken from the literature report of an LFP | LLZO | Li cell that uses a sputtered Sn interlayer to decrease the interfacial resistance between the lithium metal anode and the garnet electrolyte[36] (referred to hereafter as the "LLZO-Sn" cell). Upon insertion of Sn into the cell stack, the resultant increase in cell capacity (+16 mAh/g) decreased total cell cost by $16/kWh (cost reductions are indicated in green). This cost savings, however, is ultimately offset by the cost to deposit the Sn interlayer itself (~$23/kWh, cost increases are indicated in red). In our model, the Sn cost is especially conservative, reflecting merely the price of tin metal and not the added cost of fabricating it into a sputtering target. Thus, while inclusion of the Sn interlayer increased the performance of the cell, the associated cost savings were ultimately negated by the high cost of the materials and processing to achieve those performance gains. Our model LPSCl cell offers a contrasting example. Upon the addition of just 1 wt% binder to the composite cathode, an increase in performance of approximately 65 mAh/g was observed. This represents a cost reduction of $309/kWh. The cost to implement this change, however, amounted to less than $1/kWh, yielding a total net reduction in cost of approximately $308/kWh, more than 99% of the cost savings captured by the increase in cell capacity. These examples illustrate that it is often not clear or intuitive how materials choices will impact overall cell cost. Seemingly promising design choices and interfacial mitigations that increase cell performance can be, practically speaking, negated by their high manufacturing costs. On the other hand, even simple design choices—such as the use of an appropriate binder to enhance interfacial contact between cathode and electrolyte particles—can provide an extremely low cost pathway to large capacity gains that, in turn, yield considerable reductions in total cell cost.

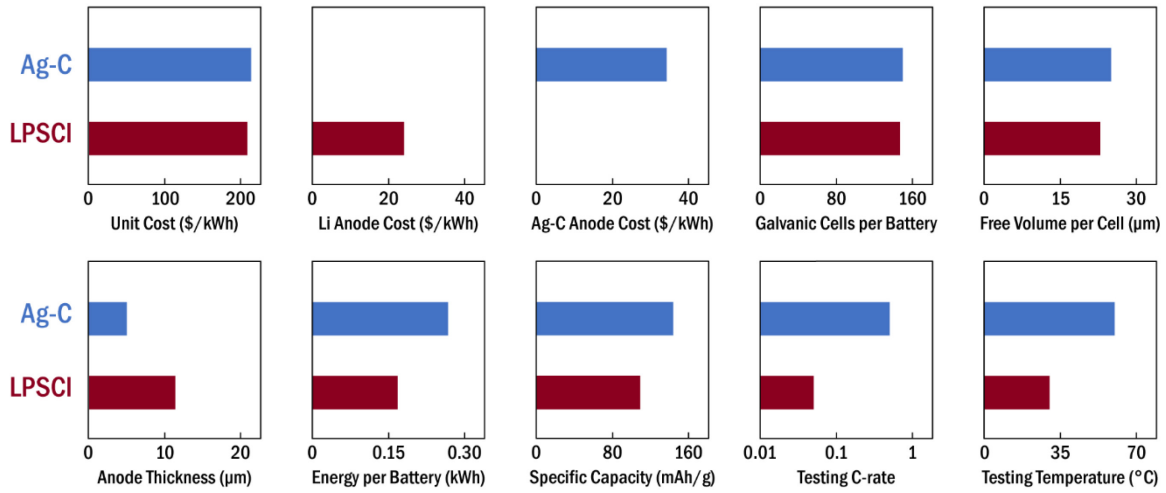

Fig. 4. Consequences of materials choice
Manufacturing cost of Ag-C and LPSCl model cells as well as comparisons between the two cells for several key underlying consequences of the disparity in anode materials selection. Specific capacity is based on active material mass in the cathode.

Finally, in Fig. 4, we illustrate multiple consequences of a difference in anode materials selection and how they ultimately contribute to overall manufacturing cost. Here we compare our previous LPSCl model cell with another example based on the recent report of a cell (also utilizing an Li_6PS_5Cl electrolyte) in which excess Li foil is instead replaced by a thin Ag-C nanocomposite layer[114] (referred to hereafter as the "Ag-C" cell). This report serves as a valuable, additional example of the key performance-processing tradeoffs under discussion here while using a contemporary, high performing, large format pouch cell fabricated with traditional battery and fuel cell slurry coating processes similar to those in our model. The total manufacturing cost of both cells is remarkably similar, despite numerous key underlying disparities that result from this difference in anode materials choice. For example, while both cells utilize Li_6PS_5Cl electrolyte and Ni-rich NMC cathode active materials, the Ag-C cell contains no excess lithium foil. The $24/kWh cost savings captured by the lack of lithium, however, is exceeded by the $34/kWh materials and processing cost of incorporating a Ag-C anode layer in its place. Moreover, both batteries can accommodate a similar number of galvanic cells in their cell stacks, a consequence of their comparable free volume requirements and the relatively small difference in thickness between the Ag-C anode layer and the excess lithium foil used in the LPSCl cell. Critically, however, the higher specific capacity exhibited by the Ag-C cell (due, in part, to a slightly higher cathode active material loading and the use of applied pressure during cycle testing) serves to offset the higher cost of the Ag-C layer as a replacement for traditional lithium foil. It is important to note here that the literature reported capacities for these two cells were recorded at different testing conditions and are, therefore, not strictly comparable. While the Ag-C cell was cycled at 0.5C, likely resulting in lower capacities than would otherwise be recorded at lower C-rates, the cell was also tested at elevated temperature. Similarly, while the performance of the LPSCl cell was measured at a lower rate (0.05C), it was tested at a comparatively lower temperature as well. Thus, while the capacities of these two cells aren't directly comparable, they are included here to illustrate how the numerous, sometimes divergent, effects of even a single materials choice (in this case, the anode) must be collectively weighed. Moreover, these capacities were measured at C-rates and temperatures with offsetting effects on cell performance.

This problem—finding relevant and diverse sets of "state-of-the-art" solid-state batteries with directly comparable cell design and testing data—remained a persistent challenge throughout the course of our analysis. In the absence of literature reports with equivalent or controlled cell configurations, electrode compositions, component thicknesses, and cycling conditions, manufacturing costs calculated from these specific, literature reported cell design and performance data cannot be meaningfully compared across reports. This reflects a much broader concern in the battery literature: the lack of standardization in test cell design and characterization protocols remains a significant barrier to accurate, widespread, and insightful analysis of battery cost, manufacturability, and scalability. Without the ability to directly compare cell performance (i.e., performance captured under equivalent testing conditions) as well as the resulting costs of those cells across different reports, researchers are ill equipped to discern which materials and process solutions are truly promising and worthy of subsequent attention. Greater benchmarking and standardization[115–117] would serve the community well.

Final Thoughts

We end by reviewing the combined effects of the three factors we've discussed in this Perspective: (1) the availability and scaling capacity of the chosen materials' constituents, (2) the cost of processing the chosen materials into full cells at high volume and yield, and (3) the performance that may be practically extracted from those materials. Take, for example, Fig. 3d, which presents the relative effects of these three factors for our model LPSCl cell. As already discussed, the cost impacts of a materials choice (in this case, a binder) are presented. Use of the binder significantly increased cell capacity while the materials and manufacturing costs for its incorporation were marginal. Moreover, by constructing and modeling a process flow in which the cell layers are calendered, we've already embodied a key aspect of the mechanical properties that drive sulfide solid electrolyte processing. Finally, to integrate the effects of materials availability, we illustrate how the price volatility of cobalt impacts cell cost. Since the Li_6PS_5Cl electrolyte doesn't appear to suffer from any considerable materials availability constraints, we examined the sensitivity of the NMC cathode to its constituent metals. For example, an increase in cobalt price approximately equal to recent cobalt price volatility[68] yielded an increase in our NMC cost of less than \$1/kg, an expected result given that prior work has already illustrated the relative insensitivity of Ni-rich NMC to the price of cobalt[80]. This small increase in NMC price increased total cell cost by ~\$1.50/kWh. Ultimately, when the collective effects of these drivers were considered, gains in performance were found to far outweigh the attendant materials and manufacturing costs or the possible cost increases due to materials availability constraints.

Scrutiny of any of these elements in isolation would have failed to capture the comprehensive understanding necessary to inform scale up. Low cost and high performance cells might fail to scale if materials supply chains are severely and unpredictably constrained. Likewise, high performance cells made from readily available materials might fail to scale if the properties of those materials require that costly or challenging manufacturing processes be used during cell integration. Collective examination of the numerous, sometimes conflicting, consequences of materials choice, for both the electrolyte and its interfacial mitigations, is necessary to accurately weigh the various key tradeoffs that are likely to drive the manufacturing and scale up of solid-state batteries.

While the present analysis makes clear the importance of using low cost materials and processes to capture large gains in cell performance, the practical realization of this strategy may be challenging. It is not clear whether the requisite ore processing and refining capacity will be able to scale at historically unprecedented rates, or whether historical and availability driven volatility in the underlying materials prices will continue. Further complicating matters, without significant additional increases in cell capacity over what has already been reported in the literature, materials supply and growth requirements will remain historically

unprecedented and possibly unattainable. Higher cell energy density serves to reduce not only the overall manufacturing costs for each kWh produced, but critically, it also reduces the mass of material required to produce each kWh (i.e., the materials intensity). It is therefore not sufficient to focus solely on increasing materials supply or on enhancing cell capacity, these drivers are coupled and must be jointly improved.

Despite these challenges, recently published work offers several promising pathways that align with aspects of our current analysis. Higher voltage charging of current NMC and LCO cathode materials enabled by high-voltage-stable electrolytes or coating materials[118], novel cathode chemistries with higher energy content[119], and higher loading densities in the composite cathode[120] could significantly boost the attainable specific capacities. Moreover, if such materials can be incorporated into full battery cells inexpensively—for instance, through rapid and low cost processing routes[121]—practical, large scale manufacturing of all-solid-state batteries could indeed be realized.

Acknowledgments

We acknowledge the MIT Energy Initiative Low Carbon Energy Center on Storage for seed funding to initiate this work. We also acknowledge contributions from Shell, materials availability graphical inspiration from Prof. Robert Jaffe, expert feedback from Dr. Rahul Malik, and data mining assistance from Brooks Clingman. This work was supported in part by the Assistant Secretary for Energy Efficiency and Renewable Energy, Vehicle Technologies Office, of the U.S. Department of Energy under Contract No. DE-AC02-05CH11231 (to G.C.), under the Advanced Battery Materials Research (BMR) Program.

References

1. International Energy Outlook 2019 (2019). (U.S. Department of Energy).

2. Goldie-Scot, L. (2019). A Behind the Scenes Take on Lithium-ion Battery Prices. https://about.bnef.com/blog/behind-scenes-take-lithium-ion-battery-prices/.

3. Zhao, N., Khokhar, W., Bi, Z., Shi, C., Guo, X., Fan, L.-Z., and Nan, C.-W. (2019). Solid Garnet Batteries. Joule *3*, 1190–1199.

4. Chan, C.K., Yang, T., and Mark Weller, J. (2017). Nanostructured Garnet-type Li7La3Zr2O12: Synthesis, Properties, and Opportunities as Electrolytes for Li-ion Batteries. Electrochimica Acta *253*, 268–280.

5. Dai, J., Yang, C., Wang, C., Pastel, G., and Hu, L. (2018). Interface Engineering for Garnet-Based Solid-State Lithium-Metal Batteries: Materials, Structures, and Characterization. Adv. Mater. *30*, 1802068.

6. Liu, Q., Geng, Z., Han, C., Fu, Y., Li, S., He, Y., Kang, F., and Li, B. (2018). Challenges and perspectives of garnet solid electrolytes for all solid-state lithium batteries. Journal of Power Sources *389*, 120–134.

7. Samson, A.J., Hofstetter, K., Bag, S., and Thangadurai, V. (2019). A bird's-eye view of Li-stuffed garnet-type $Li_7La_3Zr_2O_{12}$ ceramic electrolytes for advanced all-solid-state Li batteries. Energy Environ. Sci. *12*, 2957–2975.

8. Shoji, M., Cheng, E.J., Kimura, T., and Kanamura, K. (2019). Recent progress for all solid state battery using sulfide and oxide solid electrolytes. J. Phys. D: Appl. Phys. *52*, 103001.

9. Xiao, Y., Wang, Y., Bo, S.-H., Kim, J.C., Miara, L.J., and Ceder, G. (2019). Understanding interface stability in solid-state batteries. Nat Rev Mater.

10. Lau, J., DeBlock, R.H., Butts, D.M., Ashby, D.S., Choi, C.S., and Dunn, B.S. (2018). Sulfide Solid Electrolytes for Lithium Battery Applications. Adv. Energy Mater. *8*, 1800933.

11. Zheng, F., Kotobuki, M., Song, S., Lai, M.O., and Lu, L. (2018). Review on solid electrolytes for all-solid-state lithium-ion batteries. Journal of Power Sources *389*, 198–213.

12. Fan, L., Wei, S., Li, S., Li, Q., and Lu, Y. (2018). Recent Progress of the Solid-State Electrolytes for High-Energy Metal-Based Batteries. Adv. Energy Mater. *8*, 1702657.

13. Ma, Z., Xue, H.-G., and Guo, S.-P. (2018). Recent achievements on sulfide-type solid electrolytes: crystal structures and electrochemical performance. J Mater Sci *53*, 3927–3938.

14. Zhang, Z., Shao, Y., Lotsch, B., Hu, Y.-S., Li, H., Janek, J., Nazar, L.F., Nan, C.-W., Maier, J., Armand, M., et al. (2018). New horizons for inorganic solid state ion conductors. Energy Environ. Sci. *11*, 1945–1976.

15. Pervez, S.A., Cambaz, M.A., Thangadurai, V., and Fichtner, M. (2019). Interface in Solid-State Lithium Battery: Challenges, Progress, and Outlook. ACS Appl. Mater. Interfaces *11*, 22029–22050.

16. Bachman, J.C., Muy, S., Grimaud, A., Chang, H.-H., Pour, N., Lux, S.F., Paschos, O., Maglia, F., Lupart, S., Lamp, P., et al. (2016). Inorganic Solid-State Electrolytes for Lithium Batteries: Mechanisms and Properties Governing Ion Conduction. Chem. Rev. *116*, 140–162.

17. Lian, P.-J., Zhao, B.-S., Zhang, L.-Q., Xu, N., Wu, M.-T., and Gao, X.-P. (2019). Inorganic sulfide solid electrolytes for all-solid-state lithium secondary batteries. J. Mater. Chem. A *7*, 20540–20557.

18. Park, K.H., Bai, Q., Kim, D.H., Oh, D.Y., Zhu, Y., Mo, Y., and Jung, Y.S. (2018). Design Strategies, Practical Considerations, and New Solution Processes of Sulfide Solid Electrolytes for All-Solid-State Batteries. Adv. Energy Mater. *8*, 1800035.

19. Lee, H., Oh, P., Kim, J., Cha, H., Chae, S., Lee, S., and Cho, J. (2019). Advances and Prospects of Sulfide All-Solid-State Lithium Batteries via One-to-One Comparison with Conventional Liquid Lithium Ion Batteries. Adv. Mater. *31*, 1900376.

20. Zhao, Q., Stalin, S., Zhao, C.-Z., and Archer, L.A. (2020). Designing solid-state electrolytes for safe, energy-dense batteries. Nat Rev Mater.

21. Manthiram, A., Yu, X., and Wang, S. (2017). Lithium battery chemistries enabled by solid-state electrolytes. Nat Rev Mater *2*, 16103.

22. Xia, S., Wu, X., Zhang, Z., Cui, Y., and Liu, W. (2019). Practical Challenges and Future Perspectives of All-Solid-State Lithium-Metal Batteries. Chem *5*, 753–785.

23. Gao, Z., Sun, H., Fu, L., Ye, F., Zhang, Y., Luo, W., and Huang, Y. (2018). Promises, Challenges, and Recent Progress of Inorganic Solid-State Electrolytes for All-Solid-State Lithium Batteries. Adv. Mater. *30*, 1705702.

24. Meesala, Y., Jena, A., Chang, H., and Liu, R.-S. (2017). Recent Advancements in Li-Ion Conductors for All-Solid-State Li-Ion Batteries. ACS Energy Lett. *2*, 2734–2751.

25. Sun, C., Liu, J., Gong, Y., Wilkinson, D.P., and Zhang, J. (2017). Recent advances in all-solid-state rechargeable lithium batteries. Nano Energy *33*, 363–386.

26. Wu, Z., Xie, Z., Yoshida, A., Wang, Z., Hao, X., Abudula, A., and Guan, G. (2019). Utmost limits of various solid electrolytes in all-solid-state lithium batteries: A critical review. Renewable and Sustainable Energy Reviews *109*, 367–385.

27. Huang, K.J., Li, L., and Olivetti, E.A. (2018). Designing for Manufacturing Scalability in Clean Energy Research. Joule *2*, 1642–1647.

28. Park, K., Yu, B.-C., Jung, J.-W., Li, Y., Zhou, W., Gao, H., Son, S., and Goodenough, J.B. (2016). Electrochemical Nature of the Cathode Interface for a Solid-State Lithium-Ion Battery: Interface between $LiCoO_2$ and Garnet-$Li_7La_3Zr_2O_{12}$. Chem. Mater. *28*, 8051–8059.

29. Han, F., Yue, J., Chen, C., Zhao, N., Fan, X., Ma, Z., Gao, T., Wang, F., Guo, X., and Wang, C. (2018). Interphase Engineering Enabled All-Ceramic Lithium Battery. Joule *2*, 497–508.

30. Cai, M., Lu, Y., Su, J., Ruan, Y., Chen, C., Chowdari, B.V.R., and Wen, Z. (2019). In Situ Lithiophilic Layer from H^+/Li^+ Exchange on Garnet Surface for the Stable Lithium-Solid Electrolyte Interface. ACS Appl. Mater. Interfaces *11*, 35030–35038.

31. Lu, Z., Yu, J., Wu, J., Effat, M.B., Kwok, S.C.T., Lyu, Y., Yuen, M.M.F., and Ciucci, F. (2019). Enabling room-temperature solid-state lithium-metal batteries with fluoroethylene carbonate-modified plastic crystal interlayers. Energy Storage Materials *18*, 311–319.

32. Hu, B., Yu, W., Xu, B., Zhang, X., Liu, T., Shen, Y., Lin, Y.-H., Nan, C.-W., and Li, L. (2019). An in Situ-Formed Mosaic Li_7Sn_3/LiF Interface Layer for High-Rate and Long-Life Garnet-Based Lithium Metal Batteries. ACS Appl. Mater. Interfaces *11*, 34939–34947.

33. Wu, J., Li, X., Zhao, Y., Liu, L., Qu, W., Luo, R., Chen, R., Li, Y., and Chen, Q. (2018). Interface engineering in solid state Li metal batteries by quasi-2D hybrid perovskites. J. Mater. Chem. A *6*, 20896–20903.

34. Han, X., Gong, Y., Fu, K. (Kelvin), He, X., Hitz, G.T., Dai, J., Pearse, A., Liu, B., Wang, H., Rubloff, G., et al. (2017). Negating interfacial impedance in garnet-based solid-state Li metal batteries. Nature Mater *16*, 572–579.

35. Liu, K., Zhang, R., Wu, M., Jiang, H., and Zhao, T. (2019). Ultra-stable lithium plating/stripping in garnet-based lithium-metal batteries enabled by a SnO2 nanolayer. Journal of Power Sources *433*, 226691.

36. He, M., Cui, Z., Chen, C., Li, Y., and Guo, X. (2018). Formation of self-limited, stable and conductive interfaces between garnet electrolytes and lithium anodes for reversible lithium cycling in solid-state batteries. J. Mater. Chem. A *6*, 11463–11470.

37. Lu, Y., Huang, X., Ruan, Y., Wang, Q., Kun, R., Yang, J., and Wen, Z. (2018). An *in situ* element permeation constructed high endurance Li–LLZO interface at high current densities. J. Mater. Chem. A *6*, 18853–18858.

38. Lou, J., Wang, G., Xia, Y., Liang, C., Huang, H., Gan, Y., Tao, X., Zhang, J., and Zhang, W. (2020). Achieving efficient and stable interface between metallic lithium and garnet-type solid electrolyte through a thin indium tin oxide interlayer. Journal of Power Sources *448*, 227440.

39. Fu, K. (Kelvin), Gong, Y., Liu, B., Zhu, Y., Xu, S., Yao, Y., Luo, W., Wang, C., Lacey, S.D., Dai, J., et al. (2017). Toward garnet electrolyte–based Li metal batteries: An ultrathin, highly effective, artificial solid-state electrolyte/metallic Li interface. Sci. Adv. *3*, e1601659.

40. Luo, W., Gong, Y., Zhu, Y., Li, Y., Yao, Y., Zhang, Y., Fu, K.K., Pastel, G., Lin, C.-F., Mo, Y., et al. (2017). Reducing Interfacial Resistance between Garnet-Structured Solid-State Electrolyte and Li-Metal Anode by a Germanium Layer. Adv. Mater. *29*, 1606042.

41. Ruan, Y., Lu, Y., Huang, X., Su, J., Sun, C., Jin, J., and Wen, Z. (2019). Acid induced conversion towards a robust and lithiophilic interface for Li–Li $_{7}$ La $_{3}$ Zr $_{2}$ O $_{12}$ solid-state batteries. J. Mater. Chem. A *7*, 14565–14574.

42. Liu, K., Li, Y., Zhang, R., Wu, M., Huang, B., and Zhao, T. (2019). Facile Surface Modification Method To Achieve an Ultralow Interfacial Resistance in Garnet-Based Li Metal Batteries. ACS Appl. Energy Mater. *2*, 6332–6340.

43. Zhang, Z., Chen, S., Yang, J., Wang, J., Yao, L., Yao, X., Cui, P., and Xu, X. (2018). Interface Re-Engineering of Li $_{10}$ GeP $_{2}$ S $_{12}$ Electrolyte and Lithium anode for All-Solid-State Lithium Batteries with Ultralong Cycle Life. ACS Appl. Mater. Interfaces *10*, 2556–2565.

44. Zhao, F., Liang, J., Yu, C., Sun, Q., Li, X., Adair, K., Wang, C., Zhao, Y., Zhang, S., Li, W., et al. (2020). A Versatile Sn-Substituted Argyrodite Sulfide Electrolyte for All-Solid-State Li Metal Batteries. Adv. Energy Mater., 1903422.

45. Liu, G., Xie, D., Wang, X., Yao, X., Chen, S., Xiao, R., Li, H., and Xu, X. (2019). High air-stability and superior lithium ion conduction of Li3+3P1-Zn S4-O by aliovalent substitution of ZnO for all-solid-state lithium batteries. Energy Storage Materials *17*, 266–274.

46. Woo, J.H., Travis, J.J., George, S.M., and Lee, S.-H. (2015). Utilization of Al $_2$ O $_3$ Atomic Layer Deposition for Li Ion Pathways in Solid State Li Batteries. J. Electrochem. Soc. *162*, A344–A349.

47. Zhou, C., Samson, A.J., Hofstetter, K., and Thangadurai, V. (2018). A surfactant-assisted strategy to tailor Li-ion charge transfer interfacial resistance for scalable all-solid-state Li batteries. Sustainable Energy Fuels *2*, 2165–2170.

48. Wang, C., Gong, Y., Liu, B., Fu, K., Yao, Y., Hitz, E., Li, Y., Dai, J., Xu, S., Luo, W., et al. (2017). Conformal, Nanoscale ZnO Surface Modification of Garnet-Based Solid-State Electrolyte for Lithium Metal Anodes. Nano Lett. *17*, 565–571.

49. Tsai, C.-L., Roddatis, V., Chandran, C.V., Ma, Q., Uhlenbruck, S., Bram, M., Heitjans, P., and Guillon, O. (2016). Li $_7$ La $_3$ Zr $_2$ O $_{12}$ Interface Modification for Li Dendrite Prevention. ACS Appl. Mater. Interfaces *8*, 10617–10626.

50. Fu, K.K., Gong, Y., Fu, Z., Xie, H., Yao, Y., Liu, B., Carter, M., Wachsman, E., and Hu, L. (2017). Transient Behavior of the Metal Interface in Lithium Metal-Garnet Batteries. Angew. Chem. Int. Ed. *56*, 14942–14947.

51. Takada, K., Ohta, N., Zhang, L., Fukuda, K., Sakaguchi, I., Ma, R., Osada, M., and Sasaki, T. (2008). Interfacial modification for high-power solid-state lithium batteries. Solid State Ionics *179*, 1333–1337.

52. Sakuda, A., Hayashi, A., and Tatsumisago, M. (2010). Interfacial Observation between LiCoO $_2$ Electrode and Li $_2$ S−P $_2$ S $_5$ Solid Electrolytes of All-Solid-State Lithium Secondary Batteries Using Transmission Electron Microscopy †. Chem. Mater. *22*, 949–956.

53. Machida, N., Kashiwagi, J., Naito, M., and Shigematsu, T. (2012). Electrochemical properties of all-solid-state batteries with ZrO2-coated LiNi1/3Mn1/3Co1/3O2 as cathode materials. Solid State Ionics *225*, 354–358.

54. Okada, K., Machida, N., Naito, M., Shigematsu, T., Ito, S., Fujiki, S., Nakano, M., and Aihara, Y. (2014). Preparation and electrochemical properties of LiAlO 2 -coated Li(Ni 1/3 Mn 1/3 Co 1/3)O 2 for all-solid-state batteries. Solid State Ionics *255*, 120–127.

55. Ito, S., Fujiki, S., Yamada, T., Aihara, Y., Park, Y., Kim, T.Y., Baek, S.-W., Lee, J.-M., Doo, S., and Machida, N. (2014). A rocking chair type all-solid-state lithium ion battery adopting Li2O–ZrO2 coated LiNi0.8Co0.15Al0.05O2 and a sulfide based electrolyte. Journal of Power Sources *248*, 943–950.

56. Ohta, N., Takada, K., Sakaguchi, I., Zhang, L., Ma, R., Fukuda, K., Osada, M., and Sasaki, T. (2007). LiNbO3-coated LiCoO2 as cathode material for all solid-state lithium secondary batteries. Electrochemistry Communications *9*, 1486–1490.

57. Woo, J.H., Trevey, J.E., Cavanagh, A.S., Choi, Y.S., Kim, S.C., George, S.M., Oh, K.H., and Lee, S.-H. (2012). Nanoscale Interface Modification of $LiCoO_2$ by Al_2O_3 Atomic Layer Deposition for Solid-State Li Batteries. J. Electrochem. Soc. *159*, A1120–A1124.

58. Ohta, S., Komagata, S., Seki, J., Saeki, T., Morishita, S., and Asaoka, T. (2013). All-solid-state lithium ion battery using garnet-type oxide and Li3BO3 solid electrolytes fabricated by screen-printing. Journal of Power Sources *238*, 53–56.

59. Liu, T., Ren, Y., Shen, Y., Zhao, S.-X., Lin, Y., and Nan, C.-W. (2016). Achieving high capacity in bulk-type solid-state lithium ion battery based on Li 6.75 La 3 Zr 1.75 Ta 0.25 O 12 electrolyte: Interfacial resistance. Journal of Power Sources *324*, 349–357.

60. Schnell, J., Knörzer, H., Imbsweiler, A.J., and Reinhart, G. (2020). Solid versus Liquid—A Bottom-Up Calculation Model to Analyze the Manufacturing Cost of Future High-Energy Batteries. Energy Technol., 1901237.

61. Schnell, J., Tietz, F., Singer, C., Hofer, A., Billot, N., and Reinhart, G. (2019). Prospects of production technologies and manufacturing costs of oxide-based all-solid-state lithium batteries. Energy Environ. Sci. *12*, 1818–1833.

62. Alonso, E., Sherman, A.M., Wallington, T.J., Everson, M.P., Field, F.R., Roth, R., and Kirchain, R.E. (2012). Evaluating Rare Earth Element Availability: A Case with Revolutionary Demand from Clean Technologies. Environ. Sci. Technol. *46*, 3406–3414.

63. Kim, E., Huang, K., Saunders, A., McCallum, A., Ceder, G., and Olivetti, E. (2017). Materials Synthesis Insights from Scientific Literature via Text Extraction and Machine Learning. Chem. Mater. *29*, 9436–9444.

64. Kim, E., Huang, K., Jegelka, S., and Olivetti, E. (2017). Virtual screening of inorganic materials synthesis parameters with deep learning. npj Comput Mater *3*, 53.

65. Jensen, Z., Kim, E., Kwon, S., Gani, T.Z.H., Román-Leshkov, Y., Moliner, M., Corma, A., and Olivetti, E. (2019). A Machine Learning Approach to Zeolite Synthesis Enabled by Automatic Literature Data Extraction. ACS Cent. Sci., acscentsci.9b00193.

66. Kim, E., Huang, K., Kononova, O., Ceder, G., and Olivetti, E. (2019). Distilling a Materials Synthesis Ontology. Matter *1*, 8–12.

67. Rubayyat Mahbub, Kevin Huang, Zach Jensen, Zachary D. Hood, Jennifer L.M. Rupp, and Elsa Olivettia (2020). Text Mining for Processing Conditions of Solid-State Battery Electrolytes. Electrochemistry Communications *submitted*.

68. Olivetti, E.A., Ceder, G., Gaustad, G.G., and Fu, X. (2017). Lithium-Ion Battery Supply Chain Considerations: Analysis of Potential Bottlenecks in Critical Metals. Joule *1*, 229–243.

69. New Energy Outlook 2019 https://about.bnef.com/new-energy-outlook/.

70. Capital Markets Day 2018 https://www.umicore.com/en/cases/capital-markets-day-2018.

71. International Energy Agency (2019). Global EV Outlook 2019: Scaling-up the transition to electric mobility (OECD).

72. Mineral Commodity Summaries (2019). (U.S. Geological Survey).

73. Nassar, N.T., Graedel, T.E., and Harper, E.M. (2015). By-product metals are technologically essential but have problematic supply. Sci. Adv. *1*, e1400180.

74. Fu, X., Polli, A., and Olivetti, E. (2019). High-Resolution Insight into Materials Criticality: Quantifying Risk for By-Product Metals from Primary Production. Journal of Industrial Ecology *23*, 452–465.

75. Thomas, C. (2017). 2017 Minerals Yearbook: Germanium (U.S. Geological Survey).

76. Kavlak, G., McNerney, J., Jaffe, R.L., and Trancik, J.E. (2015). Metal production requirements for rapid photovoltaics deployment. Energy Environ. Sci. *8*, 1651–1659.

77. Gaines, L., Richa, K., and Spangenberger, J. (2018). Key issues for Li-ion battery recycling. MRS energy sustain. *5*, E14.

78. Fu, X., Beatty, D.N., Gaustad, G.G., Ceder, G., Roth, R., Kirchain, R.E., Bustamante, M., Babbitt, C., and Olivetti, E.A. (2020). Perspectives on Cobalt Supply through 2030 in the Face of Changing Demand. Environ. Sci. Technol. *54*, 2985–2993.

79. Fu, X., Schuh, C.A., and Olivetti, E.A. (2017). Materials selection considerations for high entropy alloys. Scripta Materialia *138*, 145–150.

80. Hsieh, I.-Y.L., Pan, M.S., Chiang, Y.-M., and Green, W.H. (2019). Learning only buys you so much: Practical limits on battery price reduction. Applied Energy *239*, 218–224.

81. Wolfenstine, J., Allen, J.L., Sakamoto, J., Siegel, D.J., and Choe, H. (2018). Mechanical behavior of Li-ion-conducting crystalline oxide-based solid electrolytes: a brief review. Ionics *24*, 1271–1276.

82. Ni, J.E., Case, E.D., Sakamoto, J.S., Rangasamy, E., and Wolfenstine, J.B. (2012). Room temperature elastic moduli and Vickers hardness of hot-pressed LLZO cubic garnet. J Mater Sci *47*, 7978–7985.

83. McGrogan, F.P., Swamy, T., Bishop, S.R., Eggleton, E., Porz, L., Chen, X., Chiang, Y.-M., and Van Vliet, K.J. (2017). Compliant Yet Brittle Mechanical Behavior of Li_2S-P_2S_5 Lithium-Ion-Conducting Solid Electrolyte. Adv. Energy Mater. *7*, 1602011.

84. Kerman, K., Luntz, A., Viswanathan, V., Chiang, Y.-M., and Chen, Z. (2017). Review—Practical Challenges Hindering the Development of Solid State Li Ion Batteries. J. Electrochem. Soc. *164*, A1731–A1744.

85. Riphaus, N., Strobl, P., Stiaszny, B., Zinkevich, T., Yavuz, M., Schnell, J., Indris, S., Gasteiger, H.A., and Sedlmaier, S.J. (2018). Slurry-Based Processing of Solid Electrolytes: A Comparative Binder Study. J. Electrochem. Soc. *165*, A3993–A3999.

86. Janek, J., and Zeier, W.G. (2016). A solid future for battery development. Nat Energy *1*, 16141.

87. Fu, Z., and Roosen, A. (2015). Shrinkage of Tape Cast Products During Binder Burnout. J. Am. Ceram. Soc. *98*, 20–29.

88. Jiang, Z., Wang, S., Chen, X., Yang, W., Yao, X., Hu, X., Han, Q., and Wang, H. (2019). Tape-Casting $Li_{0.34}La_{0.56}TiO_3$ Ceramic Electrolyte Films Permit High Energy Density of Lithium–Metal Batteries. Adv. Mater., 1906221.

89. Jiménez, R., del Campo, A., Calzada, M.L., Sanz, J., Kobylianska, S.D., Solopan, S.O., and Belous, A.G. (2016). Lithium $La_{0.57}Li_{0.33}TiO_3$ Perovskite and $Li_{1.3}Al_{0.3}Ti_{1.7}(PO_4)_3$ Li-NASICON Supported Thick Films Electrolytes Prepared by Tape Casting Method. J. Electrochem. Soc. *163*, A1653–A1659.

90. Jiménez, R., del Campo, A., Calzada, M.L., Sanz, J., Kobylianska, S.D., Liniova, B.O., Belous, A.G., and Ragulya, A.V. (2018). Improved conductivity in tape casted Li-NASICON supported thick films: Effect of temperature treatments and lamination. Journal of the European Ceramic Society *38*, 1679–1687.

91. Jonson, R.A., and McGinn, P.J. (2018). Tape casting and sintering of Li7La3Zr1.75Nb0.25Al0.1O12 with Li3BO3 additions. Solid State Ionics *323*, 49–55.

92. Okubo, K., Wang, H., Hayashi, K., Inada, M., Enomoto, N., Hasegawa, G., Osawa, T., and Takamura, H. (2018). A dense NASICON sheet prepared by tape-casting and low temperature sintering. Electrochimica Acta *278*, 176–181.

93. Ren, L., Luo, X., and Zhou, H. (2018). The tape casting process for manufacturing low-temperature co-fired ceramic green sheets: A review. J Am Ceram Soc *101*, 3874–3889.

94. Schröckert, F., Schiffmann, N., Bucharsky, E.C., Schell, K.G., and Hoffmann, M.J. (2018). Tape casted thin films of solid electrolyte Lithium-Lanthanum-Titanate. Solid State Ionics *328*, 25–29.

95. Vizgalov, V.A., Lukovkina, A.R., Itkis, D.M., and Yashina, L.V. (2019). Tape-casted liquid-tight lithium-conductive membranes for advanced lithium batteries. J Mater Sci *54*, 8531–8541.

96. Wang, H., Hasegawa, G., Akiyama, Y., Yamamoto, T., Inoishi, A., Akamatsu, H., Inada, M., Ishihara, T., and Hayashi, K. (2019). A highly conductive Na3V2(PO4)3 ceramic sheet prepared by tape-casting method. Electrochimica Acta *305*, 197–203.

97. Yu, H.-C., Taha, D., Thompson, T., Taylor, N.J., Drews, A., Sakamoto, J., and Thornton, K. (2019). Deformation and stresses in solid-state composite battery cathodes. Journal of Power Sources *440*, 227116.

98. Nam, Y.J., Oh, D.Y., Jung, S.H., and Jung, Y.S. (2018). Toward practical all-solid-state lithium-ion batteries with high energy density and safety: Comparative study for electrodes fabricated by dry- and slurry-mixing processes. Journal of Power Sources *375*, 93–101.

99. QuantumScape Investor Presentation (2020). https://www.quantumscape.com/wp-content/uploads/2020/09/QuantumScape-Investor-Presentation-Sept2020.pdf.

100. Choi, D., Donnelly, N., Holme, T., Hudson, W., Iyer, S., Karpenko, O., Singh, M., and Winoto, A. (2018). Garnet materials for Li secondary batteries and methods of making and using garnet materials.

101. Holme, T., and Donnelly, N. (2018). Garnet materials for Li secondary batteries and methods of making and using garnet materials.

102. Holme, T., Donnelly, N., Iyer, S., Winoto, A., Singh, M., Hudson, W., Choi, D., Karpenko, O., and Kerman, K. (2017). Garnet materials for Li secondary batteries and methods of making and using garnet materials.

103. Holme, T., Donnelly, N., Iyer, S., Winoto, A., Singh, M., Hudson, W., Choi, D., and Karpenko, O. (2019). Garnet materials for Li secondary batteries and methods of making and using garnet materials.

104. Cheng, L., Iyer, S., Gardner, W., Holme, T., Li, S., Chao, C., Donnelly, N., and Allenic, A. (2018). Annealed garnet electrolyte separators.

105. Iyer, S., Holme, T., and Donnelly, N. (2018). Lithium stuffed garnet setter plates for solid electrolyte fabrication.

106. Schnell, J., Günther, T., Knoche, T., Vieider, C., Köhler, L., Just, A., Keller, M., Passerini, S., and Reinhart, G. (2018). All-solid-state lithium-ion and lithium metal batteries – paving the way to large-scale production. Journal of Power Sources *382*, 160–175.

107. Shirouzu, N., and Lienert, P. (2020). Exclusive: Tesla's secret batteries aim to rework the math for electric cars and the grid. https://www.reuters.com/article/us-autos-tesla-batteries-exclusive-idUSKBN22Q1WC.

108. Cost and Price Metrics for Automotive Lithium-Ion Batteries (2017). (U.S. Department of Energy).

109. Ren, Y., Liu, T., Shen, Y., Lin, Y., and Nan, C.-W. (2017). Garnet-type oxide electrolyte with novel porous-dense bilayer configuration for rechargeable all-solid-state lithium batteries. Ionics *23*, 2521–2527.

110. Liu, B., Zhang, L., Xu, S., McOwen, D.W., Gong, Y., Yang, C., Pastel, G.R., Xie, H., Fu, K., Dai, J., et al. (2018). 3D lithium metal anodes hosted in asymmetric garnet frameworks toward high energy density batteries. Energy Storage Materials *14*, 376–382.

111. Yang, C., Zhang, L., Liu, B., Xu, S., Hamann, T., McOwen, D., Dai, J., Luo, W., Gong, Y., Wachsman, E.D., et al. (2018). Continuous plating/stripping behavior of solid-state lithium metal anode in a 3D ion-conductive framework. Proc Natl Acad Sci USA *115*, 3770–3775.

112. Xu, S., McOwen, D.W., Wang, C., Zhang, L., Luo, W., Chen, C., Li, Y., Gong, Y., Dai, J., Kuang, Y., et al. (2018). Three-Dimensional, Solid-State Mixed Electron–Ion Conductive Framework for Lithium Metal Anode. Nano Lett. *18*, 3926–3933.

113. Zhang, J., Zhong, H., Zheng, C., Xia, Y., Liang, C., Huang, H., Gan, Y., Tao, X., and Zhang, W. (2018). All-solid-state batteries with slurry coated LiNi0.8Co0.1Mn0.1O2 composite cathode and Li6PS5Cl electrolyte: Effect of binder content. Journal of Power Sources *391*, 73–79.

114. Lee, Y.-G., Fujiki, S., Jung, C., Suzuki, N., Yashiro, N., Omoda, R., Ko, D.-S., Shiratsuchi, T., Sugimoto, T., Ryu, S., et al. (2020). High-energy long-cycling all-solid-state lithium metal batteries enabled by silver–carbon composite anodes. Nat Energy *5*, 299–308.

115. Cao, Y., Li, M., Lu, J., Liu, J., and Amine, K. (2019). Bridging the academic and industrial metrics for next-generation practical batteries. Nat. Nanotechnol. *14*, 200–207.

116. Chen, S., Niu, C., Lee, H., Li, Q., Yu, L., Xu, W., Zhang, J.-G., Dufek, E.J., Whittingham, M.S., Meng, S., et al. (2019). Critical Parameters for Evaluating Coin Cells and Pouch Cells of Rechargeable Li-Metal Batteries. Joule *3*, 1094–1105.

117. Randau, S., Weber, D.A., Kötz, O., Koerver, R., Braun, P., Weber, A., Ivers-Tiffée, E., Adermann, T., Kulisch, J., Zeier, W.G., et al. (2020). Benchmarking the performance of all-solid-state lithium batteries. Nat Energy *5*, 259–270.

118. Nakamura, T., Amezawa, K., Kulisch, J., Zeier, W.G., and Janek, J. (2019). Guidelines for All-Solid-State Battery Design and Electrode Buffer Layers Based on Chemical Potential Profile Calculation. ACS Appl. Mater. Interfaces *11*, 19968–19976.

119. Clément, R.J., Lun, Z., and Ceder, G. (2020). Cation-disordered rocksalt transition metal oxides and oxyfluorides for high energy lithium-ion cathodes. Energy Environ. Sci. *13*, 345–373.

120. Shi, T., Tu, Q., Tian, Y., Xiao, Y., Miara, L.J., Kononova, O., and Ceder, G. (2020). High Active Material Loading in All-Solid-State Battery Electrode via Particle Size Optimization. Adv. Energy Mater. *10*, 1902881.

121. Wang, C., Ping, W., Bai, Q., Cui, H., Hensleigh, R., Wang, R., Brozena, A.H., Xu, Z., Dai, J., Pei, Y., et al. (2020). A general method to synthesize and sinter bulk ceramics in seconds. Science *368*, 521–526.